Vol 18 No 7, July 2009
1674-1056/2009/18(07)/2945-08

Chinese Physics B

© 2009 Chin. Phys. Soc.
and IOP Publishing Ltd

Electronic structure and optical properties of Nb-doped Sr_2TiO_4 by density function theory calculation*

Yun Jiang-Ni(贠江妮)† and Zhang Zhi-Yong(张志勇)‡

School of Information Science and Technology, Northwest University, Xi'an 710127, China

(Received 30 November 2008; revised manuscript received 17 December 2008)

This paper investigates the effect of Nb doping on the electronic structure and optical properties of Sr_2TiO_4 by the first-principles calculation of plane wave ultra-soft pseudo-potential based on density functional theory (DFT). The calculated results reveal that due to the electron doping, the Fermi level shifts into conduction bands(CBs) for $Sr_2Nb_xTi_{1-x}O_4$ with $x = 0.125$ and the system shows n-type degenerate semiconductor features. Sr_2TiO_4 exhibits optical anisotropy in its main crystal axes, and the *c*-axis shows the most suitable crystal growth direction for obtaining a wide transparent region. The optical transmittance is higher than 90% in the visible range for $Sr_2Nb_{0.125}Ti_{0.875}O_4$.

Keywords: density functional theory, Sr_2TiO_4, Nb-doping, electronic structure
PACC: 7115M, 7125, 7155, 7850

1. Introduction

The exploration of materials for transparent conducting oxides (TCOs) has been an urgent task because of the rapid expansion of industrial uses of TCOs films in liquid crystal displays, organic light emitting diodes and solar cells.[1−3] In particular, this is compounded by the increasing potential new uses for TCOs films[4−6] (e.g. the transparent field-effect transistor) and a resource problem for Sn-doped In_2O_3 (ITO),[2,3] which is a typical TCO and the most widely used.

Perovskite oxide and its two dimensional perovskite layered structure are attractive candidates for TCOs films. Recently, by ionic substitution and carrier doping, TCOs films with the perovskite structure have been explored both experimentally and theoretically,[7−16] and a few of them including La, Sb and In-doped $SrTiO_3$, Nb-doped $CaTiO_3$, Cd_3TeO_6, Sb-doped $SrSnO_3$, La and Sb-doped $BaSnO_3$ have been obtained in experiment.[7−13] Wang *et al*[7] have demonstrated that Sb-doped $SrTiO_3$ thin films epitaxially grown on $SrTiO_3$(001) substrates by pulsed laser deposition show good optical transmittance in the visible range. Guo H Z *et al*[9] have reported the optical properties of p-type $SrIn_xTi_{1-x}O_3$ ($x = 0.1$ and 0.2) films prepared by laser molecular beam epitaxy under different oxygen pressures and the films are highly transparent in most of the visible region. Moreover, the effect of Nb doping on the electronic and optical properties of $SrTiO_3$ has been studied by Guo X G *et al*[14] using *ab initio* linear muffin-tin orbital methods in the atomic sphere approximation. Zhang *et al*[15] have investigated the electronic structure and optical properties of In-doped $SrTiO_3$ by density functional theory (DFT) calculation. To our knowledge, however, the investigation of the layered perovskite structures, which have the potential to maintain the favourable electronic properties and exhibit similar electron transport properties of perovskite oxides for TCOs materials, is rare. So it is necessary to use the first-principles method to explore the effect of carrier doping on the electronic structure and optical properties of layered perovskite oxides.

In this paper, we perform the first-principles calculation to investigate the effect of n-type doping Nb on the perovskite layered structure Sr_2TiO_4 by the CASTEP[17] software package based on DFT. From these results, a better understanding of the electronic structure and optical properties of Nb-doped Sr_2TiO_4 with sufficient details can be estimated, and some helpful instructions can be provided for the growth of TCOs films with the layered perovskite structure.

*Project supported by the Natural Science Foundation of ShaanXi Province of China (Grant No 2005F06) and Northwest University (NWU) Graduate Innovation and Creativity Funds (Grant No 08YZZ47).
†E-mail: niniyun_hy@tom.com
‡Corresponding author. E-mail: zhangzy@nwu.edu.cn

2. Computational details

The layered perovskite-type $SrO(SrTiO_3)_n$ ($n = 1, 2, \ldots, \infty$) constitutes the prototype of the Ruddlesden–Popper phase.[18] If n is infinite (∞), the compound is cubic perovskite metal oxide $SrTiO_3$. For $n = 1$, the crystal structure of Sr_2TiO_4 is of the tetragonal K_2NiF_4 type with the space group $I4/mmm$ and its lattice constant is $a = b = 0.3885$ nm, $c = 1.260$ nm at room temperature.[19] Figure 1 shows the schematic structure of Sr_2TiO_4, which can be regarded as the alternative stacking of perovskite $SrTiO_3$ layers and SrO rock-salt-type layers along the c-axis. There are two different Ti–O bonds in the Sr_2TiO_4 system: the shorter Ti–O_a in the ab plane and the longer Ti-O_c along the c-axis. The unit cell contains two formula units of Sr_2TiO_4. In order to study fractional substitution, it is necessary to consider a larger cell than the basic unit. Thus we construct a supercell of four unit cells consisting of 56 atoms in the basis. Replacing any one of the Ti atoms by a Nb atom in the supercell will correspond to the formula $Sr_2Nb_{0.125}Ti_{0.875}O_4$ or $Sr_2Nb_xTi_{1-x}O_4$ with $x = 0.125$.

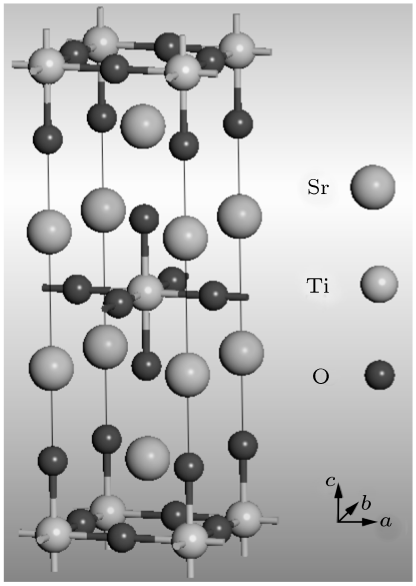


Fig.1. The schematic structure of Sr_2TiO_4.

In our calculation, the interaction between nuclei and electrons is approximated with the Vanderbilt ultra-soft pseudo-potential[20] and the Perdew and Wang 91 parametrization[21] is taken as the exchange-correlation potential in the generalized-gradient approximation (GGA). Plane wave basis with kinetic energy cutoff of 420 eV is used to represent wavefunctions. The Brillouin zone integration are approximated by using the special k-points sampling scheme of Monkhorst–Pack[22] and $6 \times 6 \times 2$ k-points grid is used. In order to obtain a stable structure, full relaxation is performed for doped Sr_2TiO_4 systems by using the Broyden-Fletcher-Goldfarb-Shanno (BFGS) algorithm[23] to minimize energy with respect to the atomic position and each calculation is considered to be converged when the maximum root-mean-square convergent tolerance is less than 1×10^{-5} eV/atom. Then the electronic structure and optical properties are calculated based on the optimized supercell model.

3. Results and discussion

3.1. Structure characterization

The fully relaxed structure parameters and single point energies of the optimized $Sr_2Nb_xTi_{1-x}O_4$ with $x = 0.0$ and $x = 0.125$ are listed in Table 1. It is clearly seen that the single point energy of Nb-doped Sr_2TiO_4 increases after doping, indicating that Nb-doped Sr_2TiO_4 is less stable than undoped Sr_2TiO_4. This is because the radius of Nb^{5+} (0.064 nm) is larger than that of Ti^{4+} (0.0605 nm), and the substitution of Nb^{5+} for Ti^{4+} results in crystal lattice aberration. Correspondingly, residual stress is generated in the process of crystallization, which causes repulsive interaction among redundant positive charges of Nb^{5+}. Therefore the single point energy increases. This case has also been discovered in Sn-doped In_2O_3.[24] However, it should be noticed that the crystal structure of $Sr_2Nb_xTi_{1-x}O_4$ with $x = 0.125$ is still the tetragonal K_2NiF_4 type with the space group $I4/mmm$. Moreover, after Nb doping, the calculated lattice parameter a increases, while the lattice parameter c decreases, which is in good agreement with the experimental results.[25]

Table 1. The optimized structure parameters and single point energies (E) of Sr_2TiO_4 and $Sr_2Nb_{0.125}Ti_{0.875}O_4$.

	a/Å		c/Å		c/a		E/eV
	theory	experimental	theory	experimental	theory	experimental	theory
Sr_2TiO_4	3.91	3.89[a]	12.63	12.60[a]	3.23	3.24[a]	–10110.1459
$Sr_2Nb_{0.125}Ti_{0.875}O_4$	3.94	3.90[b]	12.61	12.58[b]	3.20	3.23[b]	–10096.3995

[a] Ref.[16], [b]Ref.[22].

Further insight into the effect of Nb doping on the structure of Sr_2TiO_4 system can be obtained from bond lengths surrounding the doping atom (see Table 2). And the partial geometries around the Nb atom, which are taken from the structural optimized Nb-doped 56 atom $Sr_2Nb_{0.125}Ti_{0.875}O_4$ supercell, are shown in Fig.2. Because of symmetrical constraints, atoms behave the same in the a, b directions. For undoped Sr_2TiO_4, the Ti–O_a and Ti–O_c bonds are 1.957 Å and 1.977 Å, respectively. The introduction of an Nb atom leads to a local lattice expansion and the four nearest O_a, O_b and the two second nearest O_c atoms around the Nb atom shift away from Nb by 0.028 Å and 0.007 Å, respectively. That is, the NbO_6 octahedron exhibits significant structure relaxations. In the case of its first nearest neighbour (NN) $Ti6O_6$ and $Ti7O_6$ octahedra, they exhibit smaller structure relaxations. The Ti6–O_a and Ti6–O_c bond lengths in the doped $Sr_2Nb_{0.125}Ti_{0.875}O_4$ system are 0.007 Å and 0.004 Å smaller than the corresponding ones in the undoped Sr_2TiO_4 system, respectively. At the same time, it is noted that the second NN $Ti8O_6$ octahedron undergoes few relaxations after doping. Hence, replacing a Ti atom by one Nb atom in the supercell merely results in significant local structural changes in the dopant sites.

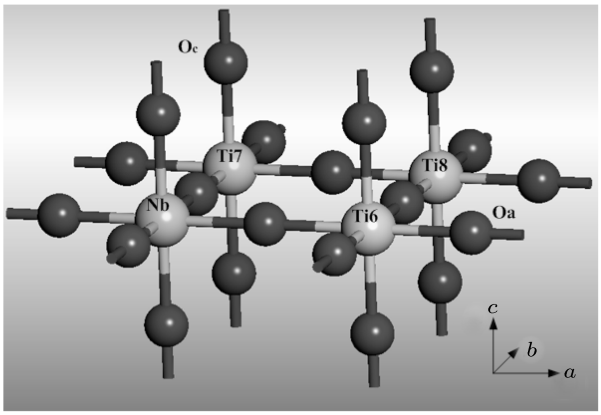


Fig.2. Partial geometry for the Nb-doped 56 atom $Sr_2Nb_{0.125}Ti_{0.875}O_4$ supercell.

Table 2. The bond lengths surrounding the doping atom Nb and the corresponding bond lengths of the undoped Sr_2TiO_4 system after structural relaxation. All quantities are in angstroms.

	Undoped Sr_2TiO_4		$Sr_2Nb_{0.125}Ti_{0.875}O_4$	
	bond	bond length	bond	bond length
	Ti–O_a	1.957	Nb–O_a	1.985(0.028)
	Ti–O_b	1.957	Nb–O_b	1.985(0.028)
	Ti–O_c	1.997	Nb–O_c	2.004(0.007)
first NN $Ti6O_6$	Ti6–O_a	1.957	Ti6–O_a	1.950(–0.007)
	Ti6–O_b	1.957	Ti6–O_b	1.950(–0.007)
	Ti6–O_c	1.997	Ti6–O_c	1.993(–0.004)
first NN $Ti7O_6$	Ti7–O_a	1.957	Ti7–O_a	1.950(–0.007)
	Ti7-O_b	1.957	Ti7–O_b	1.950(–0.007)
	Ti7–O_c	1.997	Ti7–O_c	1.993(–0.004)
second NN $Ti8O_6$	Ti8–O_a	1.957	Ti8–O_a	1.954(–0.003)
	Ti8–O_b	1.957	Ti8–O_b	1.954(–0.003)
	Ti8–O_c	1.997	Ti8–O_c	2.000(0.003)

The deviations of bond lengths between $Sr_2Nb_{0.125}Ti_{0.875}O_4$ and undoped Sr_2TiO_4 are given in parenthesis.

3.2. Electronic structures

3.2.1. Electronic structure of undoped Sr_2TiO_4

In order to show the Nb doping effect on the electronic structure of Sr_2TiO_4, the total density of states (DOS) and partial DOS (PDOS) of stoichiometric Sr_2TiO_4 are calculated first for comparison and the results are shown in Fig.3. For the sake of clarity, only the relevant Ti 3d, O_a 2p, O_c 2p and Sr 5s PDOS are shown and this will be adopted in the subsequent Fig.5(c).

It is obvious that the structure of Sr_2TiO_4 has corner-shared TiO_6 octahedra where the Ti 3d and O 2p interaction is found, which dominate the main electronic properties of Sr_2TiO_4. The top of valance bands (VBs) consists of predominately O 2p states and the most prominent unoccupied energy bands in the bottommost of conduction bands (CBs) are mainly composed of the Ti 3d states. Overlooking from the DOS, we can observe that there is strong orbital hy-

bridization between the Ti 3d and O 2p states. That is to say, the Ti–O bond is covalent. Moreover, it is of particular interest that there are two different oxygen atoms in the structure of Sr_2TiO_4 and they have different PDOS. The PDOS of O_c atoms which locate on the edge of the perovskite layer hybridize a little with that of the Ti atoms, and this indicates that the covalent interaction of Ti–O_c bonds on the edge of the perovskite layer is weaker than that of other Ti–O_a bonds. Correspondingly no overlap of PDOS between Sr atoms and O atoms means ionicity of Sr–O bonds.

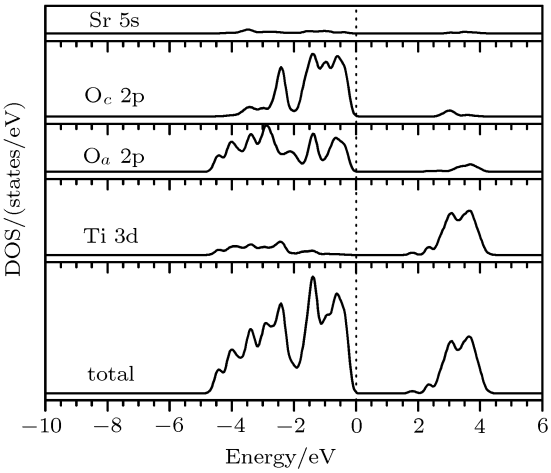


Fig.3. The DOS and PDOS of Sr_2TiO_4. The Fermi level is set to zero on the energy scale, which will be adopted below unless otherwise stated.

In addition, the calculated band gap of Sr_2TiO_4 is about 1.7eV, which is smaller than the experimental values of about 3.8 eV.[19] This is typically underestimated by the DFT[26] and also caused by the strong self-interaction of the Ti 3d states.[27]

3.2.2. Effect of Nb doping on the electronic structure

3.2.2.1. DOS

Figure 4 shows the total DOS of $Sr_2Nb_xTi_{1-x}O_4$ with $x = 0.125$. Because the Nb doping introduces the n-type carriers into the system, the Fermi level shifts into the CBs, which is in good agreement with the experimental results[25] that the $Sr_2Nb_{0.1}Ti_{0.9}O_4$ system is an n-type semiconductor. At the same time, the DOS shifts significantly towards low energy and the optical band gap broadens. The calculated optical band gap of $Sr_2Nb_{0.125}Ti_{0.875}O_4$ is about 0.6 eV larger than that of undoped Sr_2TiO_4 due to Nb doping. This can be explained as follows: on the one hand, the Burstein–Moss shift due to the high concentration of carriers makes the optical absorption edge shift towards low energy, and the optical band gap is broadened;[28] On the other hand, interactions among electric charges result in a many-body effect, which causes the optical band gap to become narrow.[29] But the effect of Burstein–Moss[28] on the band gap is more pronounced than the many-body effect, so the band gap broadens after Nb doping.

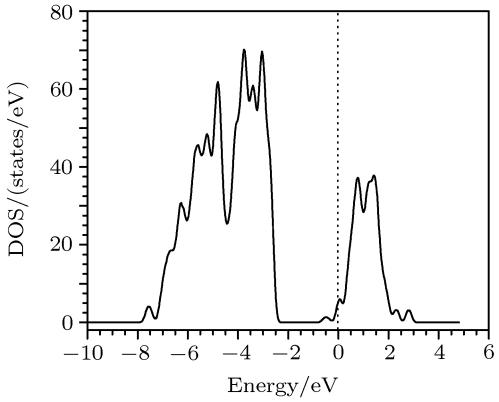


Fig.4. The DOS of $Sr_2Nb_{0.125}Ti_{0.875}O_4$.

The broadened optical band gap may be expressed by the following equation:

$$E_g = E_{go} + \Delta E_g^{BM} - \Delta E_g^{W}.$$

Here E_{go} is the band gap of undoped Sr_2TiO_4, ΔE_g^{BM} is the Burstein–Moss shift and ΔE_g^{W} is the CB change resulting from the many-body effect among electrons. Moreover, an additional small peak appears in the bottom of the VBs. We will discuss it later.

3.2.2.2. PDOS

Figure 5 shows the PDOSs of $Sr_2Nb_xTi_{1-x}O_4$ with $x = 0.0$ and 0.125, the orbital decomposed PDOSs of the Nb atom and its nearest atoms (O_a, O_c, Sr, Ti6 and Ti8 (see Fig.2)).

By analysing the PDOSs in Figs.5(b) and 5(c), we find that the VBs of the $Sr_2Nb_{0.125}Ti_{0.875}O_4$ system are mainly composed of O2p states, and the CBs is formed by Ti3d and Nb4d states, which is in good agreement with the experimental results that the electronic transport properties of the $Sr_2Nb_{0.1}Ti_{0.9}O_4$ system are dominated by the TiO_6 octahedra.[25] The calculated PDOSs of Nb, Ti6 and Ti8 in the Fermi level are 0.63, 0.74, 0.65 states/eV, respectively, which confirms that the Sr_2TiO_4 system undergoes insulator to metal transition due to Nb doping and the Nb doping has a great effect on the conductivity of $Sr_2Nb_{0.125}Ti_{0.875}O_4$.

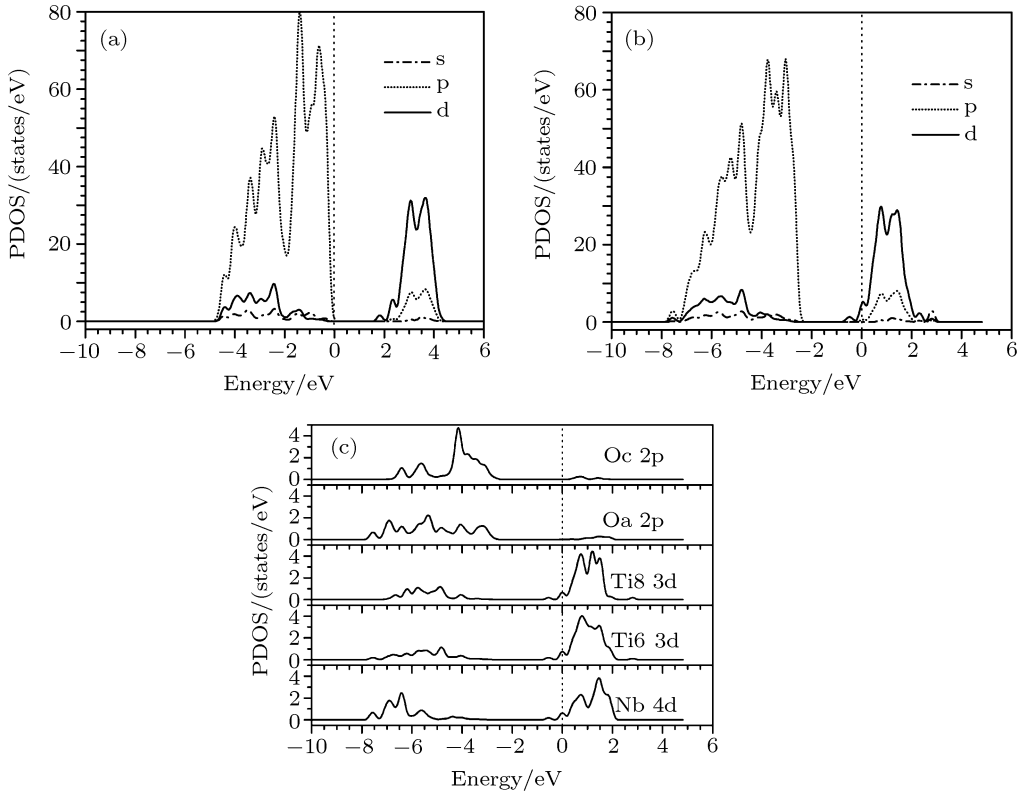


Fig.5. The (a) PDOS of Sr_2TiO_4; (b) the PDOS of $Sr_2Nb_{0.125}Ti_{0.875}O_4$; (c) the orbital decomposed PDOSs of Nb atom and its nearest atoms in $Sr_2Nb_{0.125}Ti_{0.875}O_4$.

In addition, the PDOS of $Sr_2Nb_{0.125}Ti_{0.875}O_4$ has some changes in comparison with that of Sr_2TiO_4. One additional small peak appears in the bottom of the VBs, to which the O 2p, Ti6 3d, Ti8 3d and Nb 4d states make contributions. Also the PDOS of $Sr_2Nb_{0.125}Ti_{0.875}O_4$ shifts significantly towards low energy after Nb doping, and the dispersion of the VBs are aggravated due to the high doping concentration that makes the impurity atoms become closer to each other. In this case, the wavefunctions which are bounded by the doping ions greatly overlap, resulting in enhancement of the communization movement between the O2p orbit and the impurity atom orbit, so the VBs are broadened.

The CBs are highly dispersive and show no localization characteristics after Nb doping. It is known that the effective radius of Nb^{5+} is larger than that of Ti^{4+}, the partial substitution of Nb for Ti has broken the Ti–O octahedron, which makes the unsubstituted Ti and O atoms squeeze into each other. This leads to a stronger hybridization between the Ti 3d and O 2p states, so the CBs become highly dispersive.

3.2.2.3. Electron density difference

Next, we discuss the Nb doping effect on the electronic structure of $Sr_2Nb_{0.125}Ti_{0.875}O_4$ in terms of the electron density difference. And the electron density difference of undoped Sr_2TiO_4 in the (001) plane is first calculated for comparison (see Fig.6(a)). It can be found that there is a strong covalency between Ti–O bonds in the Sr_2TiO_4 system, and the electron cloud near the Ti and O atoms indicates the orientation characteristic of covalency. Moreover, the covalent interaction of Ti–O_c bond is weaker than that of Ti–O_a bond, which further confirms the electronic structure analysis of Sr_2TiO_4 in Section 3.2.1.

After doping, the electron density difference of $Sr_2Nb_{0.125}Ti_{0.875}O_4$ in the (001) plane demonstrates a considerable electron charge density redistribution. The overlap of electron density between the Nb and O atoms shows a prominent stronger covalent bonding effect than that between the Ti and O atoms. Also the covalent interaction between Ti and O atoms in $Sr_2Nb_{0.125}Ti_{0.875}O_4$ along the c-axis is enhanced, but that along the a-axis has little change in comparison with that of undoped Sr_2TiO_4. Furthermore, the electron cloud of Ti and O atoms shifts towards low energy and the symmetry of the crystal reduces, which is consistent with

the above discussed DOS and PDOS of $Sr_2Nb_{0.125}Ti_{0.875}O_4$ system.

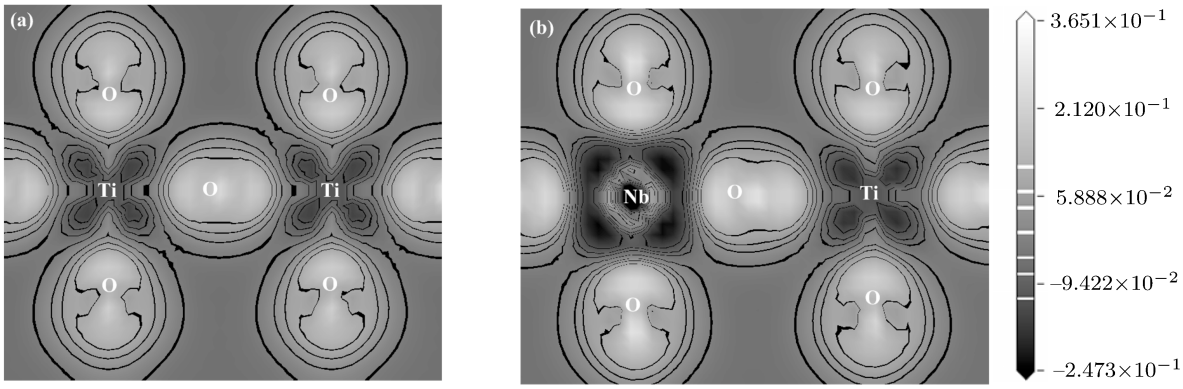


Fig.6. Electron density difference of $Sr_2Nb_xTi_{1-x}O_4$ in the (001) plane (a) $x = 0.0$; (b) $x = 0.125$.

3.3. The optical properties

Further insight into the effect of Nb doping on the electronic structure of Sr_2TiO_4 can be obtained from the calculation of optical properties. The linear response of a system due to an external electromagnetic field with a small wave vector can be described with the complex dielectric function $\varepsilon(\omega) = \varepsilon_1(\omega) + \mathrm{i}\varepsilon_2(\omega)$. The imaginary part of the dielectric function $\varepsilon_2(\omega)$ is calculated from the momentum matrix elements between the occupied and unoccupied wave function,[30]

$$\varepsilon_2(\omega) = \frac{Ve^2}{2\pi\hbar m^2\omega^2}\int \mathrm{d}^3k \sum_{n,n'} \langle kn|p|kn'\rangle|^2 f(kn) \times (1 - f(kn'))\delta(E_{kn} - E_{kn'} - \hbar\omega), \quad (1)$$

where $\hbar\omega$ is the energy of the incident photon, V is the unit cell volume, p is the momentum operator, $|kn\rangle$ is a crystal wavefunction and $f(kn)$ is the Fermi distribution function. The real part of the dielectric function $\varepsilon_1(\omega)$ is evaluated from the imaginary part $\varepsilon_2(\omega)$ by the Kramers–Kronig relationship.[31]

$$\varepsilon_1(\omega) = 1 + \frac{2}{\pi}M\int_0^\infty \frac{\varepsilon_2(\omega')\omega'}{\omega'^2 - \omega^2}\mathrm{d}\omega, \quad (2)$$

where M is the principal value of the integral. The other optical constants like refractive index $n(\omega)$, extinction coefficient $k(\omega)$, reflectivity $R(\omega)$ and absorption coefficient $I(\omega)$ now are immediately calculated in terms of the components of the complex dielectric function as follows:

$$n(\omega) = \left(\frac{1}{\sqrt{2}}\left[\sqrt{\varepsilon_1(\omega)^2 + \varepsilon_2(\omega)^2} + \varepsilon_1(\omega)\right]\right)^{1/2}, \quad (3)$$

$$k(\omega) = \left(\frac{1}{\sqrt{2}}\left[\sqrt{\varepsilon_1(\omega)^2 + \varepsilon_2(\omega)^2} - \varepsilon_1(\omega)\right]\right)^{1/2}, \quad (4)$$

$$R = \frac{(n-1)^2 + k^2}{(n+1)^2 + k^2}, \quad (5)$$

$$I = \frac{2K\omega}{c}. \quad (6)$$

Accordingly the transmittance $T(\omega)$ can be obtained by the following equation

$$T(\omega) = 1 - R(\omega) - I(\omega). \quad (7)$$

In the present work, we only show our calculated dielectric function and optical transmittance for the Sr_2TiO_4 crystal due to the fact that the two optical constants are of significant importance for transparent conducting films. The calculated polarized imaginary part of the dielectric function $\varepsilon_2(\omega)$ for Sr_2TiO_4 with

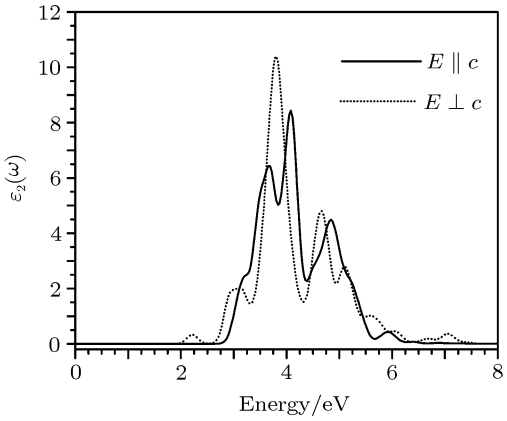


Fig.7. The calculated polarized imaginary part of the dielectric function $\varepsilon_2(\omega)$ for Sr_2TiO_4.

electric field E parallel ($E \parallel c$) and perpendicular ($E \perp c$) to the c-axis is shown in Fig.7. Obviously, the

calculated optical properties of the Sr_2TiO_4 system are anisotropic, which result from the two dimensional layered structure and are consistent with the experimental results.[16] For the calculated $E \perp c$ spectrum, the small peak emerging in the energy region of 2.0 eV to 2.5 eV and the peak around 3.0 eV are both contributed by transitions from the O_a 2p states to the Ti 3d t_{2g} states. While the high peak appearing in the energy range of 3.4 eV to 4.2 eV corresponds to the transition from O_a 2p states to the Ti 3d e_g states.

In the case of $E \parallel c$, the shoulder locating at 3.2 eV corresponds to the transition from O_c 2p states to the Ti 3d t_{2g} states. And the high peak in the energy range of 3.3 eV to 4.4 eV is due to the transition from O_c 2p states to Ti 3d e_g states. In particular, this peak is quite broad, which is due to the O_c 2p band near the Fermi level being wider than that of the O_a (see Fig.3). In addition, it should be noticed that the optical absorption edge in the case of $E \parallel c$ appears at a higher energy region than that in the $E \perp c$ spectrum. This implies that the c-axis is the most suitable crystal growth direction for obtaining the Sr_2TiO_4 material with a wide transparent region.

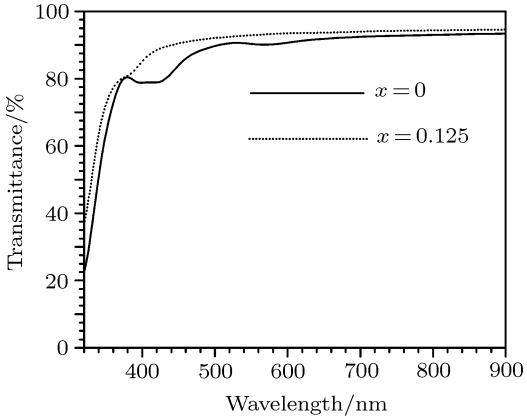


Fig.8. Optical transmittances of $Sr_2Nb_xTi_{1-x}O_4$ with $x = 0.0$ and 0.125.

Furthermore, we calculated the optical transmittance of $Sr_2Nb_xTi_{1-x}O_4$ with $x = 0.0$ and 0.125 in the case of $E \parallel c$ and the results are shown in Fig.8. Obviously the transmittance of Nb doped Sr_2TiO_4 has a significant improvement after doping and the transmittance is higher than 90% in the visible range. The increase of high transparency originates from two factors. There is no doubt that one is the wide optical band gap which broadens after doping, and the other is the low DOS in the CBs, which leads to the small transition probability and weak absorption.

So far, there is no experimental data about Nb-doped Sr_2TiO_4 transparent conducting films. However, Matsuno *et al*[19] have successfully synthesized a Sr_2TiO_4 single-crystalline thin film by pulsed laser deposition method and the target of Sr_2TiO_4 is prepared by conventional solid state reaction. Lee *et al*[25] have prepared a Nb-doped Sr_2TiO_4 ceramic sample by the standard solid state reaction. And the Sb-doped $SrSnO_3$ transparent conducting film[13] has been grown on $SrTiO_3(100)$ substrate by the pulsed laser deposition method, the ceramic target of $SrSb_{0.05}Sn_{0.95}O_3$ is prepared by the standard solid state reaction by using $SrCO_3$, SnO_2, and Sb_2O_3 powders.

Thus, by optimally controlling the Nb and Ti stoichiometry, we can expect to grow Nb-doped Sr_2TiO_4 transparent conducting films on $SrTiO_3$ (100) substrate by pulsed laser deposition using a KrF excimer laser ($\lambda = 248$ nm). The target of $Sr_2Nb_{0.125}Ti_{0.875}O_4$ can be prepared by standard solid state reactions using high purity $SrCO_3$, TiO_2, and Nb_2O_5 powders.

4. Conclusions

We have investigated the electronic band structures including the DOS, PDOS and electron density difference of $Sr_2Nb_xTi_{1-x}O_4$ with $x = 0.0$ and 0.125 by using the first-principles calculation of plane wave ultra-soft pseudo-potential based on the DFT. Due to the electron doping, the Fermi level shifts into CBs for $Sr_2Nb_xTi_{1-x}O_4$ with $x = 0.125$ and the system displays n-type degenerate semiconductor features. At the same time, the DOS shifts towards low energy and the optical band gap is broadened. Our calculations of the optical properties of Sr_2TiO_4 show a large anisotropy between $E \parallel c$ and $E \perp c$. The optical absorption edge in the case of $E \parallel c$ is occurring at a higher energy region, indicating that the c-axis is the most suitable direction of crystal growth for a wide transparent region. In addition, the optical transmittance Sr_2TiO_4 has a significant improvement after doping, the transmittance is higher than 90% in the visible range. These results indicate that Nb-doped Sr_2TiO_4 can be attractive as a new TCO with the perovskite structure.

References

[1] Kim H and Pique A 2004 *Appl. Phys. Lett.* **84** 218

[2] Furubayashi Y, Hitosugi T, Yamamoto Y, Inaba K, Kinoda G, Hirose Y, Shimada T and Hasegawa T 2005 *Appl. Phys. Lett.* **86** 252101

[3] Furubayashi Y, Yamada N, Hirose Y, Yamamoto Y, Otani M, Hitosugi T, Shimada T and Hasegawa T 2007 *J. Appl. Phys.* **101** 093705

[4] Nomura K, Ohta H, Ueda K, Kamiya T, Hirano M and Hosono H 2003 *Science* **300** 1269

[5] Kwon Y, Li Y, Heo Y W, Jones M, Holloway P H, Norton D P, Park Z V and Li S 2004 *Appl. Phys. Lett.* **84** 2685

[6] Siddiqui J, Cagin E, Chen D and Phillips J D 2006 *Appl. Phys. Lett.* **88** 212903

[7] Wang H H, Chen F, Dai S Y, Zhao T, Lu H B, Cui D F, Zhou Y L, Chen Z H and Yang G Z 2001 *Appl. Phys. Lett.* **78** 1676

[8] Cho J H and Cho H J 2001 *Appl. Phys. Lett.* **79** 1426

[9] Guo H Z, Liu L F, Fei Y Y, Xiang W F, Lu H B, Dai S Y, Zhou Y L and Chen Z H 2003 *J. Appl. Phys.* **94** 4558

[10] Wang R P and Tao C J 2002 *J. Cryst. Growth* **245** 63

[11] Tetsuka H, Shen Y J, Tezuka K, Imoto H and Wasa K 2006 *J. Vac. Sci. Technol.* A **24** L4

[12] Wang H F, Liu Q Z, Chen F, Gao G Y, Wu W and Chen X H 2007 *J. Appl. Phys.* **101** 106105

[13] Liu Q Z, Wang H F, Chen F and Wu W 2008 *J. Appl. Phys.* **103** 093709

[14] Guo X G, Chen X S and Lu W 2003 *Solid State Communications* **126** 441

[15] Zhang Z Y, Yun J N and Zhang F C 2007 *Chin. Phys.* **16** 2791

[16] Zhang C 2007 *Chin. Phys.* **16** 1422

[17] Segall M D, Lindan P J D, ProbertM J , Pickard C J, Hasnip P J, Clark S J and Payne M C 2002 *J. Phys. Conds. Matt.* **14** 2717

[18] Ruddlesden S N and Popper P 1957 *Acta Crystallogr.* **10** 538

[19] Matsuno J, Okimoto Y, Kawasaki M and TokuraY 2005 *Phys. Rev. Lett.* **95** 176404

[20] Vanderbilt D 1990 *Phys. Rev.* B **41** 7892

[21] Perdew J P, Chevary J A, Vosko S H, Jackson K A, Pederson M R, Singh D J and Fiolhais C 1992 *Phys. Rev.* B **46** 6671

[22] Monkhorst H J and Pack J D 1976 *Phys. Rev.* B **13** 5188

[23] Pfrommer B G, Cote M, LouieS G and Cohen M L 1997 *J. Comput. Phys.* **131** 233

[24] Sorescu M, Diamandescu L, Tarabsanu-Mihaila D and Teodorescu V S 2004 *J. Mater. Sci.* **39** 675

[25] Lee K H, Kim S W, Ohta H and Koumoto K 2006 *J. Appl. Phys.* **100** 063717

[26] Jones R O and Gunnarsson O 1989 *Rev. Mod. Phys.* **61** 689

[27] Wei S H and Zunger A 1988 *Phys. Rev.* B **37** 8958

[28] Burstein E 1954 *Phys. Rev.* **93** 632

[29] Mahan G D 1980 *J. Appl. Phys.* **51** 2634

[30] Saha S, Sinha T P and Mookerjee A 2000 *Phys. Rev.* B **62** 8828

[31] Shen X C 2002 *Spectrum and Optical Properties for Semiconductors* (Beijing: Science Press) (in Chinese)